Article

Effect of Process Parameters and Definition of Favorable Conditions in Multi-Material Extrusion of Bimetallic AZ31B–Ti6Al4V Billets

Daniel Fernández *, Alvaro Rodríguez-Prieto and Ana María Camacho

Department of Manufacturing Engineering, Universidad Nacional de Educación a Distancia (UNED), 28040 Madrid, Spain; alvaro.rodriguez@ind.uned.es (A.R.-P.); amcamacho@ind.uned.es (A.M.C.)

* Correspondence: dfernande146@alumno.uned.es

Abstract: This paper investigates the extrusion process to manufacture bimetallic cylinders combining a magnesium alloy core (AZ31B) and a titanium alloy sleeve (Ti6Al4V) of interest in aeronautical applications. A robust finite element model has been developed to determine the most influential parameters and to study the effect of them on the extrusion force and damage induced by means of Design of Experiments (DOE) and Taguchi method. The results show that the most influential parameters in the extrusion forces are the friction between sleeve and container/die and the height of the cylinder; and the less influential ones are the process temperature and ram speed. Moreover, minimum values of forces along with low damage can be reached by favorable interface contact conditions, minimizing the friction at the core-container/die interface, as the main influencing factor; followed by the geometrical dimensions of the billet, being the billet height more important when paying attention to the minimum forces, and being the core diameter when considering the minimum damage as the most important criterion. The results can potentially be used to improve the efficiency of this kind of extrusion process and the quality of the extruded part that, along with the use of lightweight materials, can contribute to sustainable production approaches.

Keywords: metal forming; extrusion; multi-material; bimetallic; AZ31B; Ti6Al4V; finite element method; DOE; force; damage

1. Introduction

Development of multi-material parts has gained relevance during recent years due to the possibilities of adapting the mechanical properties of each material to the specific in-service requirements of the component. Thus, by combining different materials, it is possible to achieve a weight reduction and improve stiffness and strength among other properties; formability can also be improved thanks to the combination of properties. Because of this, the industrial technologies for advanced joining and assembly processes of multi-material have been identified as a critical research and development area of the European Union (EU) Horizon 2020 work program 2018–2020 [1].

In the aerospace industry, the reduction of the weight in the components is a key factor to increase the payload in aircrafts and satellites, saving fuel and reducing the environmental impact. For these reasons, the use of composite materials, such as thermoplastic or thermosetting resins combined with carbon fiber is very well implemented. Currently, additive manufacturing is acquiring more and more importance to reduce tooling costs and manufacture parts with impossible shapes using conventional methods, among other advantages related to the sustainability [2] and design optimization [3]. Additive manufacturing techniques can also be an alternative to conventional processes when design specifications of obsolete parts are difficult to obtain due to a lack of information, such as component drawings or bill of materials, as explained by Rodríguez-Prieto et al. [4].

The problem with these kinds of multi-material components is the limitation in their in-service behavior, as composite materials cannot be used for high temperature requirements. Although additive manufacturing techniques are experiencing very quick improvements, still have poorer surface finishing and lower mechanical properties than parts made by conventional methods due to the layer by layer structure [5], the dimensions of the components to be manufactured are also limited. Furthermore, in the manufacturing of multi-material components by additive manufacturing, other factors, such as materials compatibility, formation of brittle inter-metallic metallurgical structures, residual stresses, and microstructure thermal e*ff*ects become decisive.

The co-extrusion process is typically used to obtain multi-material cylinders to be used as billets to manufacture components with complex shapes. This is a complex thermo-mechanical process due to the combination of plastic deformation and di*ff*usion in the interface of both materials because of the pressure and temperatures generated. There are several studies about the combination of Mg and Al alloys, such as the one by Negendanka et al. [6], where the influence of the die angle and di*ff*erent combining techniques of Mg–core and Al–sleeve on the di*ff*usion layer formation are investigated. Another example is the work by Thirumurugan et al. [7], where a ZM21 magnesium alloy/CP aluminum was fabricated through direct hot co-extrusion with three di*ff*erent extrusion ratios and constant temperature and ram speed. Gall et al. [8] also studied the co-extrusion of bimetallic Al–Mg billets into hollow profiles by means of experiments and Finite Element Method (FEM) simulation. Lehmann et al. [9] analyzed the mechanical strength and fracture properties of hydrostatic coextruded Al–Mg compounds. Other studies regarding multi-material co-extrusion have been performed using Cu–Al, for example, Lapovok et al. [10] studied the inter-di*ff*usion improvement in the manufacturing of Cu–Al bimetallic tubes using severe plastic deformation methods. Berski et al. [11] analyzed the strain–stress state in bimetallic rods composed by Cu–Al using two di*ff*erent extrusion ratios in conical die and in double reduction die. A study about the deformation behavior of an Al/Cu clad composite by the method of twist channel angular pressing (TCAP) was conducted by Kocich et al. [12]; whereas Rong et al. [13] studied the e*ff*ects on microstructure and mechanical properties of a Mg-Gd-Zn-Zr alloy manufactured by di*ff*erential-thermal extrusion. Alcaraz and Sevillano [14] used Finite Element (FE) calculations to study the influence of the di*ff*erent extrusion variables in the bimetallic tubes composed by two di*ff*erent Al alloys. The work of Camacho et al. [15] is another example of a multi-material forming process used in other kind of applications, such as minting. However, only a few studies have explored the behavior of such di*ff*erent metallic alloys in terms of density, tensile strength, yield strength, and elastic modules, such as by Behrens et al. [16], who performed a lateral angular co-extrusion (LACE) to product semi-finished products consisting of aluminum and steel. More information about the LACE process for the production of coaxially reinforced hollow profiles can be found in Thürer et al. [17].

In this study, the direct extrusion of a bimetallic cylinder with a magnesium alloy AZ31B core and a titanium alloy Ti6Al4V sleeve has been analyzed by means of finite element simulation and the design of experiments (DOE) technique; special attention has been paid to the forces required and damage induced in order to determine the most relevant parameters to choose the most e*ffi*cient operating conditions.

2. Materials and Methods

2.1. Materials, Geometrical Dimensions, and Process Parameters

The bimetallic cylinders used in the simulations have a magnesium alloy UNS M11311 core and a titanium alloy UNS R56400 as sleeve (Figure 1); due to their excellent properties, these alloys are well known in the industry by the nomenclature AZ31B and Ti6Al4V, respectively, so this will be the designation used in the paper from now on.

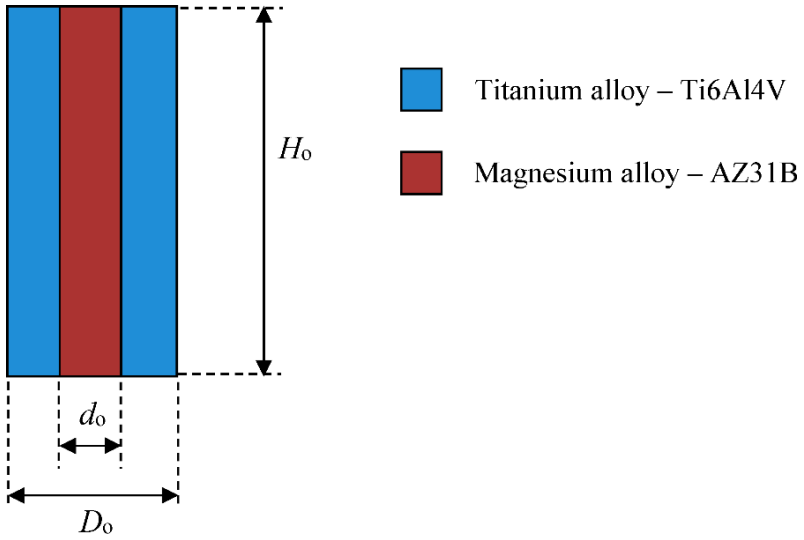

Figure 1. Bimetallic cylinder sketch and initial geometrical dimensions.

The parameters of the extrusion process considered in this work are presented in Figure 2.

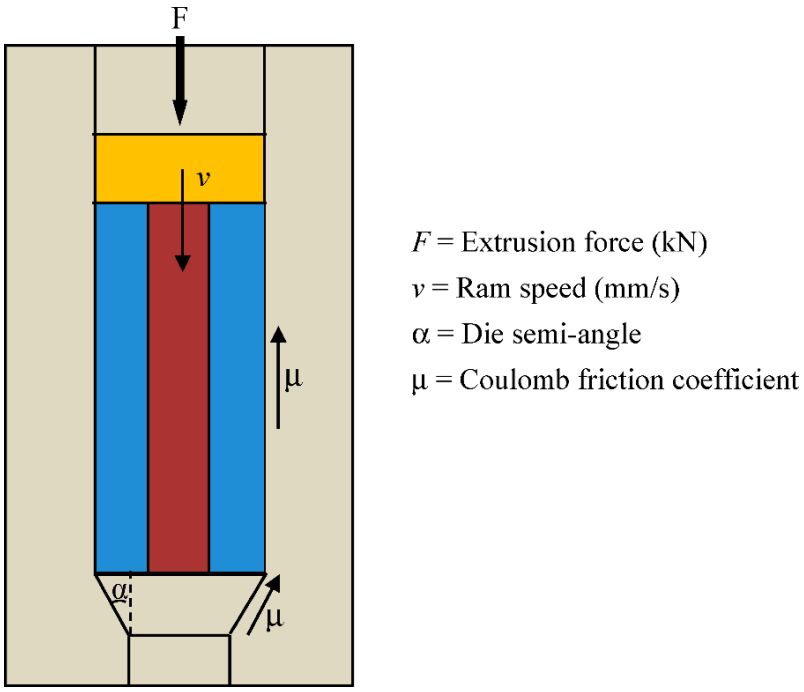

Figure 2. Extrusion process schema.

The chemical composition of both materials are listed in Table 1 [18] and Table 2 [19].

Table 1. Chemical composition of magnesium alloy AZ31B.

Material	Mg (wt.%)	Al (wt.%)	Zn (wt.%)	Mn (wt.%)	Si (wt.%)	Cu (wt.%)	Ca (wt.%)	Fe (wt.%)	Ni (wt.%)
AZ31B	97	2.5–3.5	0.6–1.4	0.20	0.1	0.05	0.04	0.005	0.005

Table 2. Chemical composition of titanium alloy Ti6Al4V.

Material	Ti (wt.%)	Al (wt.%)	V (wt.%)	Fe (wt.%)	C (wt.%)	O (wt.%)	N (wt.%)	H (wt.%)
Ti6Al4V	Bal.	5.5–6.5	3.5–4.5	0.25	0.08	0.13	0.040	0.012

The physical and mechanical properties of both materials are included in Table 3 [18,19] for comparison.

Table 3. Physical and mechanical properties of the magnesium alloy AZ31B and titanium alloy Ti6Al4V.

Property	AZ31B	Ti6Al4V
Density (g/cm^3)	1.74	4.46
Tensile strength (MPa)	260	≥895
Yield strength (MPa)	200	≥828
Elastic modulus (GPa)	44.80	105–120
Poisson's ratio	0.35	0.31

2.2. *Finite Element Modeling*

Finite element simulations were performed by the commercial finite element program DEFORM 3D. Taking advantage of the axial symmetry of the problem, only a quarter of the process has been modeled in order to reduce the computation time and other computational resources, such as storage needs. The ram and the container were modeled as rigid objects and the bimetallic cylinders were modeled as an assembly between two plastic objects (sleeve and core).

The plastic parts have been meshed using tetrahedral elements. A mesh study has been realized in order to determine the best mesh configuration. Meshes with 5000, 7000, and 13,000 elements have been considered. In Figure 3, the extrusion force results versus the die stroke are shown for different mesh sizes.

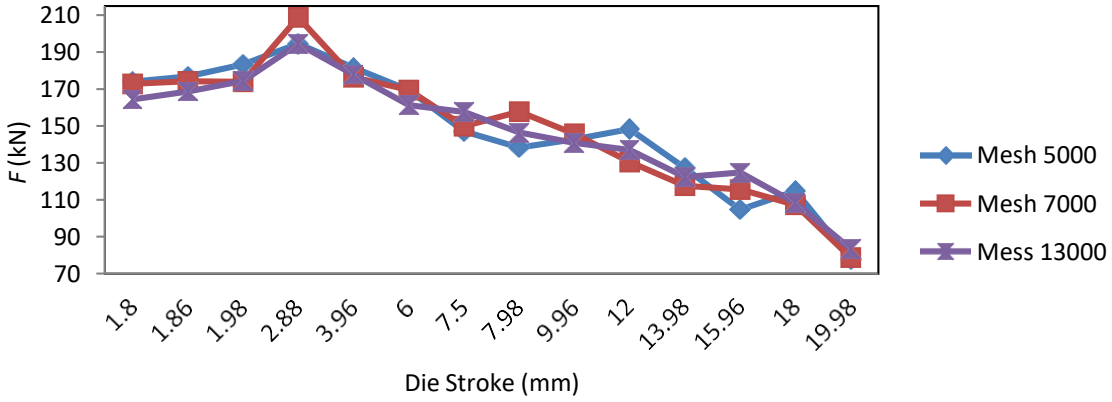

Figure 3. Extrusion force for different mesh sizes.

Taking into account that the results for the extrusion force using several mesh sizes are quite similar, 7000 elements mesh size is considered the optimum one due to the compromise between the precision reached and the computational time to perform each simulation.

The contact conditions among the different objects have to be defined as well. Rigid objects are considered "master" (the ones who deform) and the plastic objects are considered "slave" (the ones who are deformed). In the case of sleeve and core interaction, where both objects are plastic, titanium alloy is defined as "master" and magnesium alloy as "slave", according to the properties presented in Table 3. The friction model used in all the simulations is the Coulomb model that, along with the shear friction model, is one of the classical friction models in metal forming analysis [20].

Materials AZ31B and Ti6Al4V were assumed to be isotropic during all the process. The flow curves used for Ti6Al4V are from DEFORM library.

In the case of AZ31B, as there was no reference in DEFORM, an exponential model defined by Wen-Juan [21] was used to define the flow curves, obtaining the results shown in Table 4.

Table 4. AZ31B flow curves values based on Wen-Juan exponential model.

	Strain	Stress (MPa)			
		T = 150 °C	T = 200 °C	T = 250 °C	T = 300 °C
Strain rate = 0.001	0.02	112.69	91.54	74.35	60.40
	0.05	133.12	107.86	87.40	70.82
	0.10	168.45	136.07	109.91	88.78
	0.15	202.14	163.00	131.44	105.99
	0.20	230.06	185.44	149.47	120.49
	0.25	248.31	200.35	161.65	130.42
	0.30	254.18	205.56	166.23	134.43
Strain rate = 0.01	0.02	127.46	105.42	87.19	72.11
	0.05	149.13	122.70	100.95	83.06
	0.10	186.21	152.12	124.27	101.52
	0.15	221.25	179.81	146.14	118.77
	0.20	250.18	202.67	164.18	133.01
	0.25	269.21	217.81	176.23	142.58
	0.30	275.67	223.20	180.72	146.32
Strain rate = 0.1	0.02	144.17	121.41	102.25	86.11
	0.05	167.06	139.58	116.61	97.43
	0.10	205.84	170.06	140.50	116.08
	0.15	242.17	198.36	162.48	133.08
	0.20	272.07	221.51	180.34	146.83
	0.25	291.87	236.80	192.13	155.88
	0.30	298.99	242.36	196.46	159.25

Damage factor has been also used in this work as a parameter to evaluate the quality of the extrudate. Damage factor is evaluated in DEFORM using normalized Cockcroft and Latham criterion [22], typically used for predicting damage in metal forming operations [23], due to its simplicity and the accessibility of material data required for its calculation. This criterion considers that the fracture is mainly governed by the maximum principal stress, as it is shown in Equation (1):

$$\int_0^{\varepsilon_f} (\sigma_{max}/\sigma_H) d\varepsilon = C \quad (1)$$

where ε is the equivalent plastic strain, ε_f is the equivalent strain to fracture, σ_{max} is the maximum principal stress, σ_H is the stress according to the Huber–Mises hypothesis and C is a constant depending on the material and experimental determined.

2.3. Finite Element Model Validation

The FE model validation has been performed theoretically comparing the simulations results for the extrusion force with the results using Johnson semi-empirical model [24–26], typically used in this kind of analysis. In this model the deformation is defined in Equation (2):

$$\varepsilon_x = a + b \cdot ln(r_x) \quad (2)$$

where r_x is the extrusion ratio (A_0/A) and a and b are constants obtained by semi-empirical methods whose values are 0.8 and 1.2, respectively.

The extrusion force is defined in Equation (3):

$$F = A_0 \cdot \sigma_f \cdot \left(\varepsilon_x + \frac{2L}{D_0}\right) \quad (3)$$

where A_0 is the initial area, L is the contact length of the container, D_0 is the initial diameter of the billet and σ_f is the average flow stress.

Three simulations have been performed to validate the model. In all the simulations the cylinder had 12 mm of external diameter and 20 mm of height and the final external diameter was 9 mm, therefore the extrusion ratio (r_x) is 1.77. The first simulation is performed using a Ti6Al4V cylinder, the second one using a AZ31B cylinder and the last one using a bimetallic billet with a core of 6 mm diameter.

The extrusion parameters were a die semi-angle of 45°, a friction coefficient of 0.1, a ram speed of 2 mm/s and a temperature of 200 °C.

Equation (4) [27] was used to obtain the flow stress for the multi-material cylinder:

$$\sigma_m = \sigma_c \cdot \frac{V_c}{V_c + V_s} + \sigma_s \cdot \frac{V_s}{V_c + V_s} \quad (4)$$

where σ_m is the yield stress for the multi-material part, σ_c is the yield stress for the core, σ_s is the yield stress for the sleeve, V_c is the volume of the core and V_s is the volume of the sleeve.

The comparison results are shown in Figures 4–6.

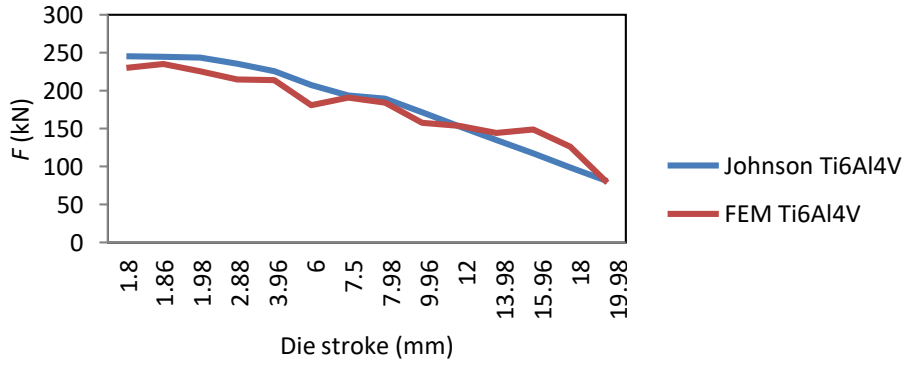

Figure 4. Comparison chart between Johnson and FEM extrusion force for a billet of Ti6Al4V.

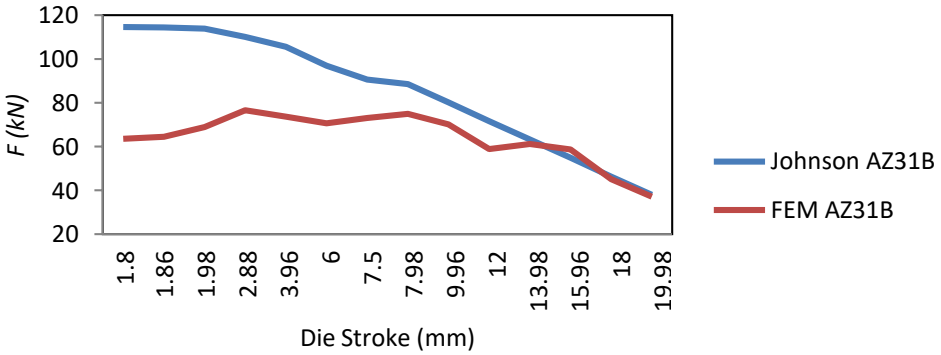

Figure 5. Comparison chart between Johnson and FEM extrusion force for a billet of AZ31B.

After comparing the analytical results with the simulation ones, it can be concluded that the FE model is robust enough to be validated.

2.4. Design of Experiments (DOE)

Once the FE model has been validated, the next step is to define the design of experiment (DOE) methodology [28] to identify and quantify the parameters with a higher influence in the extrusion force and the damage induced in the multi-material extrudate.

In Figure 7, an Ishikawa chart is shown in order to list the possible causes that may affect the extrusion force; where H_0 is the initial height of the billet, D_0 is the initial external diameter of the sleeve and d_0 is the initial diameter of the core.

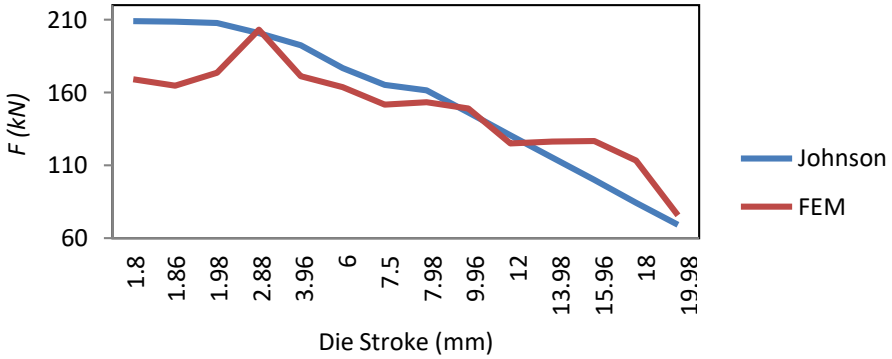

Figure 6. Comparison chart between Johnson and FEM extrusion force for a multi-material billet.

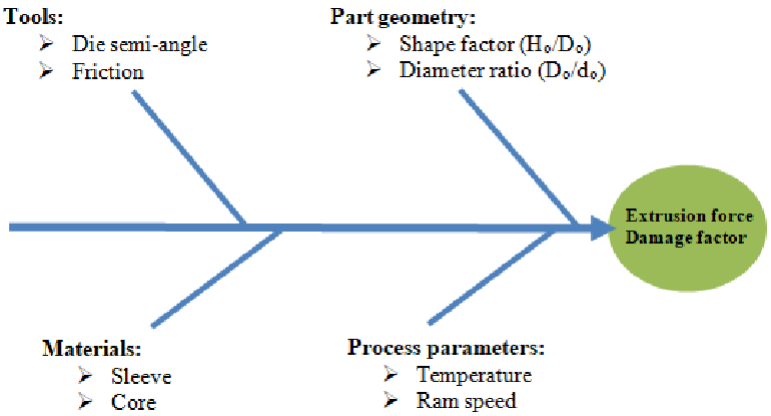

Figure 7. Ishikawa's chart for the analysis of the bimetallic extrusion process.

The values range for each cause/parameter is shown in Table 5:

Table 5. Cause/parameter values distributed by levels.

Variable	Cause/Factor	Units	Level 1	Level 2	Level 3	Level 4	Level 5
X_1	Core diameter	mm	4	5	6	7	8
X_2	Billet height	mm	12	15	20	25	30
X_3	Ram speed	mm/s	1	1.5	2	2.5	3
X_4	Temperature	°C	100	150	200	250	300
X_5	Friction coefficient	N/A	0.030	0.065	0.100	0.135	0.170
X_6	Die semi-angle	°	15	30	45	60	75

The DOE technique consists on the combination of these independent variables by fixing all the values in the center one (level 3), except the variable whose behavior wants to be known. Thus, for each of these combinations, a value for the dependent variables (extrusion force and damage factor) will be obtained.

In Tables 6–11, the combinations of these variables and their influence in the extrusion force are shown. The same procedure has been followed with the independent variable damage factor.

Table 6. Variables combination by varying X_1 (core diameter).

Simulation	X_1 (mm)	X_2 (mm)	X_3 (mm/s)	X_4 (°C)	X_5	X_6 (°)	Extrusion Force (kN)
1	**4**	20	2	200	0.1	45	249.60
2	**5**	20	2	200	0.1	45	221.25
3	**6**	20	2	200	0.1	45	207.46
4	**7**	20	2	200	0.1	45	183.65
5	**8**	20	2	200	0.1	45	165.92

Table 7. Variables combination by varying X_2 (billet height).

Simulation	X_1 (mm)	X_2 (mm)	X_3 (mm/s)	X_4 (°C)	X_5	X_6 (°)	Extrusion Force (kN)
1	6	**12**	2	200	0.1	45	180.29
2	6	**16**	2	200	0.1	45	186.55
3	6	**20**	2	200	0.1	45	207.46
4	6	**24**	2	200	0.1	45	233.23
5	6	**28**	2	200	0.1	45	278.63

Table 8. Variables combination by varying X_3 (ram speed).

Simulation	X_1 (mm)	X_2 (mm)	X_3 (mm/s)	X_4 (°C)	X_5	X_6 (°)	Extrusion Force (kN)
1	6	20	**1**	200	0.1	45	221.66
2	6	20	**1.5**	200	0.1	45	215.94
3	6	20	**2**	200	0.1	45	207.46
4	6	20	**2.5**	200	0.1	45	211.10
5	6	20	**3**	200	0.1	45	208.14

Table 9. Variables combination by varying X_4 (temperature).

Simulation	X_1 (mm)	X_2 (mm)	X_3 (mm/s)	X_4 (°C)	X_5	X_6 (°)	Extrusion Force (kN)
1	6	20	2	**100**	0.1	45	241.82
2	6	20	2	**150**	0.1	45	222.75
3	6	20	2	**200**	0.1	45	207.46
4	6	20	2	**250**	0.1	45	185.97
5	6	20	2	**300**	0.1	45	170.37

Table 10. Variables combination by varying X_5 (friction coefficient).

Simulation	X_1 (mm)	X_2 (mm)	X_3 (mm/s)	X_4 (°C)	X_5	X_6 (°)	Extrusion Force (kN)
1	6	20	2	200	**0.030**	45	136.63
2	6	20	2	200	**0.065**	45	198.06
3	6	20	2	200	**0.100**	45	207.46
4	6	20	2	200	**0.135**	45	243.50
5	6	20	2	200	**0.170**	45	276.28

3. Results

3.1. Determination of Most Influential Parameters in the Extrusion Force

After performing the simulations according to the DOE defined in the previous section, the values obtained for the extrusion force are placed in a perturbation chart (Figure 8) in order to check which parameters produce a bigger deviation between the lowest and the highest extrusion force values.

Table 11. Variables combination by varying X_6 (die semi-angle).

Simulation	X_1 (mm)	X_2 (mm)	X_3 (mm/s)	X_4 (°C)	X_5	X_6 (°)	Extrusion Force (kN)
1	6	20	2	200	0.1	**15**	164.64
2	6	20	2	200	0.1	**30**	151.71
3	6	20	2	200	0.1	**45**	207.46
4	6	20	2	200	0.1	**60**	216.34
5	6	20	2	200	0.1	**75**	226.21

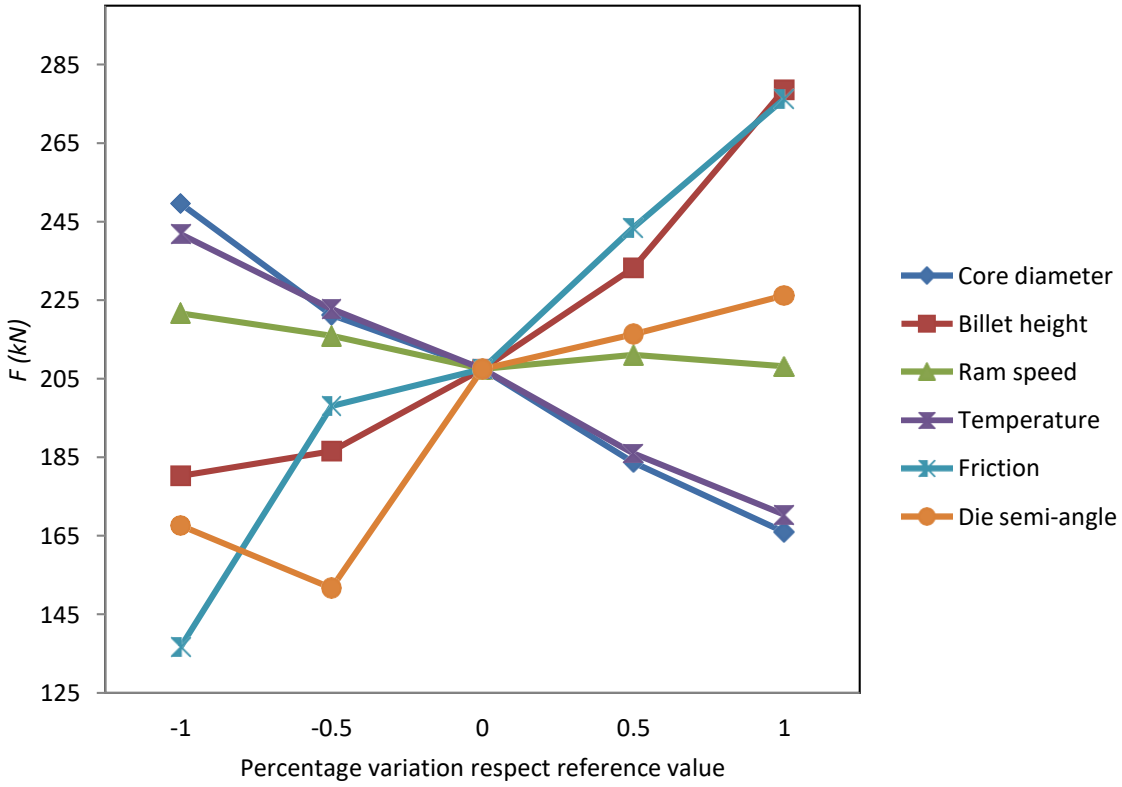

Figure 8. Perturbation chart of the bimetallic extrusion process.

In the perturbation chart shown in Figure 8, it can be verified that the most influential parameters in the extrusion force are billet height, friction, and die semi-angle. However, in the case of the temperature and the core diameter, the difference is not so clear. Therefore, in Figure 9, a percentage variation respect the reference value (level 3) of the extrusion force is shown.

The conclusion is that ram speed and temperature are the less relevant factors in the extrusion force compared to the most influential factors.

In order to classify the rest of the factors, a Taguchi's analysis of variance (ANOVA) [27] is performed. Table 12 shows the Taguchi's ortogonal array for four variables with three levels and Table 13 shows the results for the average values taking into account the criteria "the lower the best" to indicate that the best results occur when the extrusion force is the minimum.

The most relevant factor to obtain a low extrusion force during the process is the die semi-angle followed very close by the friction.

3.2. *Analysis of the Influence of the Process Parameters in the Extrusion Force*

Once it is clarified in which magnitude the extrusion force is affected by the process parameters, it is time to analyze in which way each parameter affects to the extrusion force. Figure 10 presents the results of the analysis, and they will be discussed below.

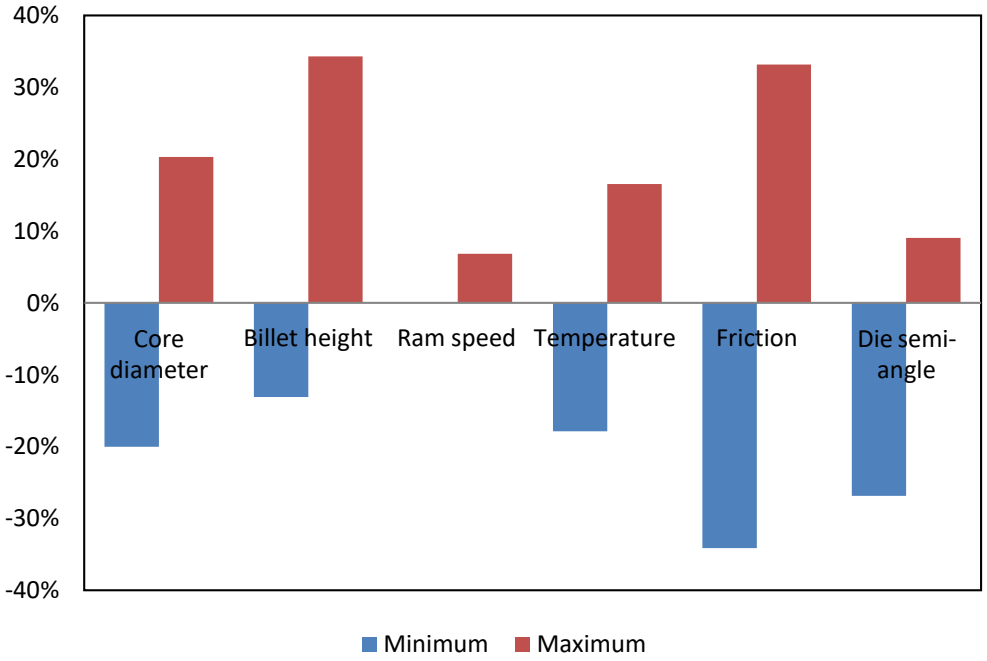

Figure 9. Percentage variation respect the reference value (level 3) of the extrusion force.

Table 12. Taguchi's orthogonal array for extrusion force.

Simulation	Core Diameter (mm)	Friction	Billet Height (mm)	Die Semi-Angle (°)	Extrusion Force (kN)
1	6	0.07	15	30	119.20
2	6	0.10	20	45	207.46
3	6	0.15	25	60	380.79
4	7	0.07	20	60	191.42
5	7	0.10	25	30	161.97
6	7	0.15	15	45	182.98
7	8	0.07	25	45	161.00
8	8	0.10	15	60	157.51
9	8	0.15	20	30	177.18

Table 13. Taguchi's results for the average values for extrusion force (kN).

Level	Core Diameter	Friction	Billet Height	Die Semi-Angle
1	235.80	157.20	153.20	152.80
2	178.80	175.60	192.00	183.80
3	165.20	247.00	234.60	243.20
Delta	70.60	89,80	81.40	90.50
Classification	4	2	3	1

3.2.1. Core Diameter

The influence of the core diameter is inversely proportional to the necessary extrusion force. As the diameter increases, the necessary force decreases as it is shown in Figure 10a.

This result is expected since as we increase the diameter of the core, the internal diameter of the ring decreases, so the volume of Ti6Al4V in the cylinder is smaller. As more force is needed to extrude the Ti6Al4V than for the AZ31B, it is logical to expect that the force necessary to extrude the multi-material cylinder will be less.

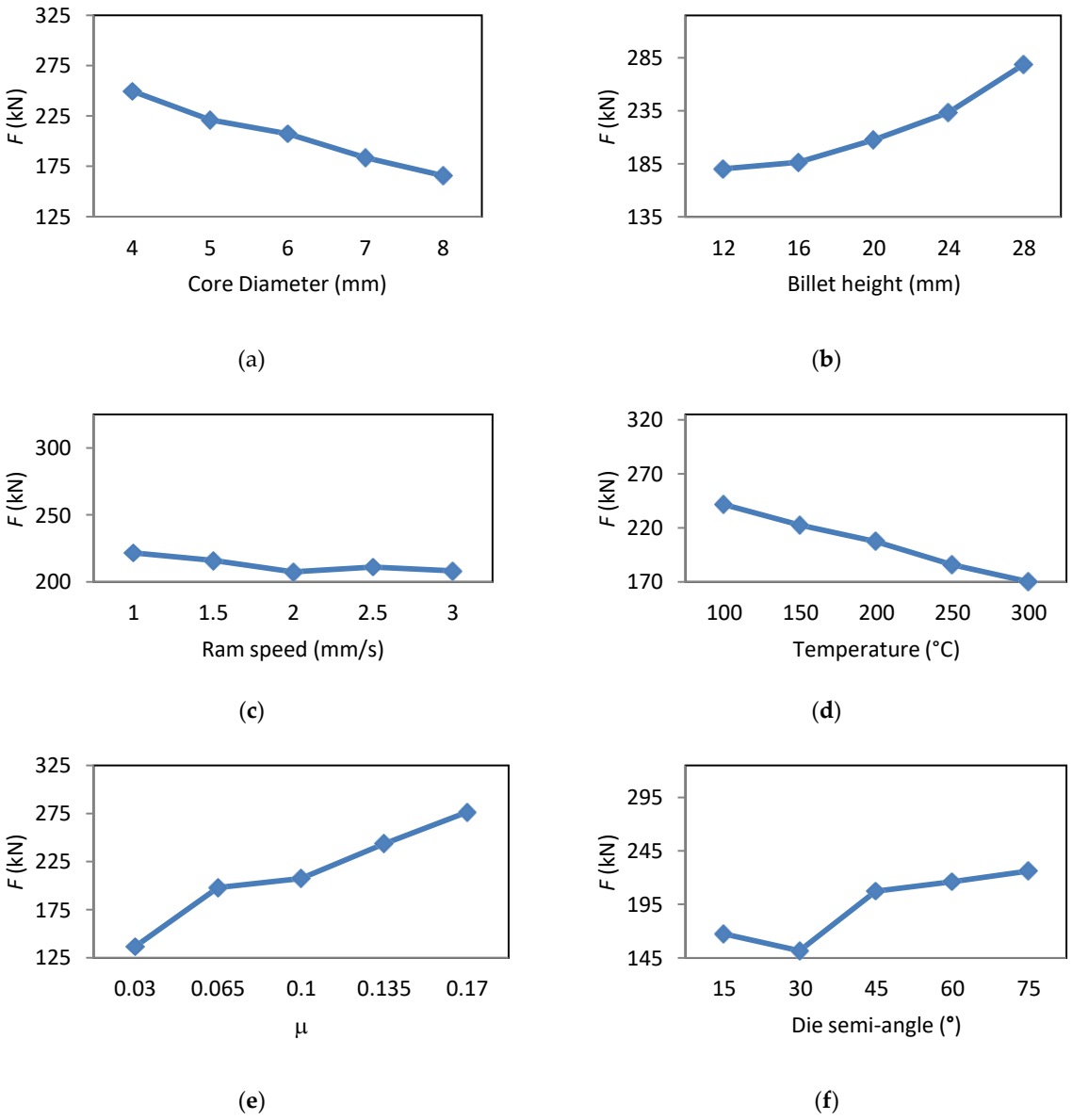

Figure 10. Influence of the parameters on the extrusion force. (**a**) *Core diameter; (**b**) *Billet height; (**c**) *Ram speed; (**d**) Temperature; (**e**) *Friction; (**f**) *Die semi-angle. *Temperature of the process is 200 °C.

3.2.2. Billet Height

Unlike the diameter of the core, as the height increases, the force required to extrude the part increases, as it can be seen in Figure 10b.

This result can be explained because as the height increases, the contact area of the billet with the container increases too; as a consequence, this causes an increase of the energy component due to friction and, therefore, of the total force required.

3.2.3. Ram Speed

The ram speed is linked to the deformation speed that will be imposed to the part during the process and it is the factor that has the least relevance in the extrusion force, resulting in a decrease with the ram speed increase as can be seen in Figure 10c.

This effect can be explained because as the ram speed increases the temperature increases due to the friction in the container/billet interface. This increase of temperature reduces the stress necessary to deform the billet and, thus, the extrusion force is lower and remains practically constant at highest speed.

Another important effect observed is that, as the speed of the die is increased, the maximum effective stress on the core decreases, until it reaches a minimum for v = 2.5 mm/s, as shown in Figure 11. This will be of interest in industrial application of extrusion processes because this has a direct influence in the quality of the extrudate.

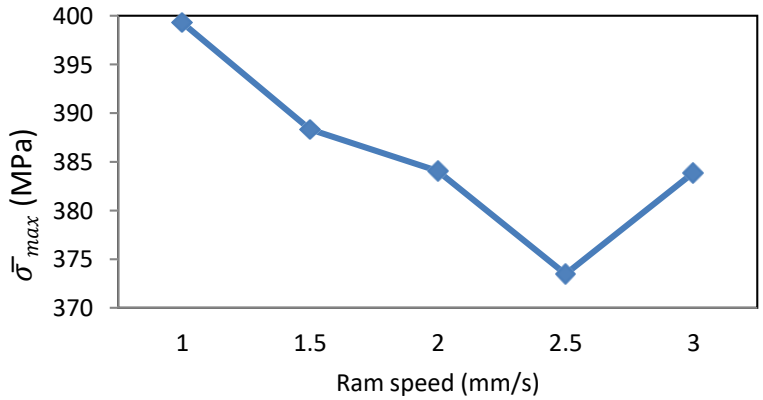

Figure 11. Influence of the ram speed on the core maximum effective stress (T = 200 °C).

3.2.4. Temperature

The process temperature has an effect inversely proportional to the extrusion force as shown in the Figure 10d. This relationship was expected by observing the flow curves of AZ31B and Ti6Al4V, because the temperature decreases the flow stress of metallic materials, and it is typically used to increase the formability of these materials. Temperature is the second parameter with the least influence on the extrusion force of the process.

For the entire temperature range, the maximum extrusion force is achieved for a die displacement of 2.88 mm. Furthermore, it is observed in Figure 12 that increasing the temperature decreases the maximum stress on the core.

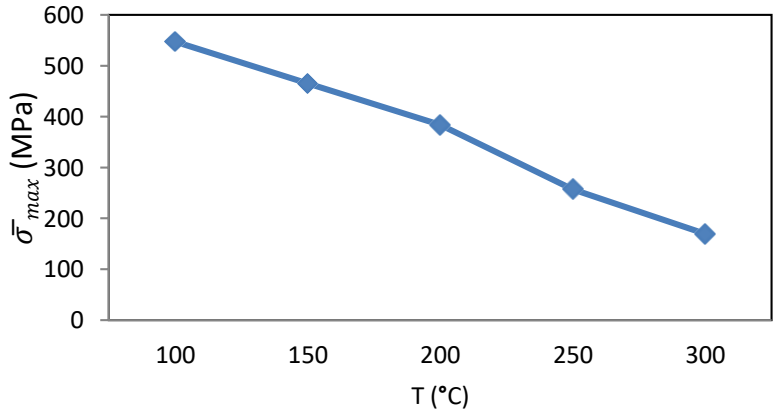

Figure 12. Influence of the temperature on the core maximum effective stress.

Temperature affects the sleeve maximum effective stress in a practically linear way, as shown in Figure 13.

3.2.5. Friction

The friction at the interface between the container and the sleeve is the second most influential factor considered on the extrusion force of the process. In this work, it has been considered that the

ring and core have been assembled with an interference fit, and due to the compression forces that they will suffer during the whole process, the friction between them would be maximum. Even so, in all of the simulations, it can be seen that there is a slip between the two at the beginning of the extrusion, being the part that always slides the AZ31B magnesium alloy. As can be seen in the graph of Figure 10e, as friction increases, the extrusion force necessary to carry out the process increases.

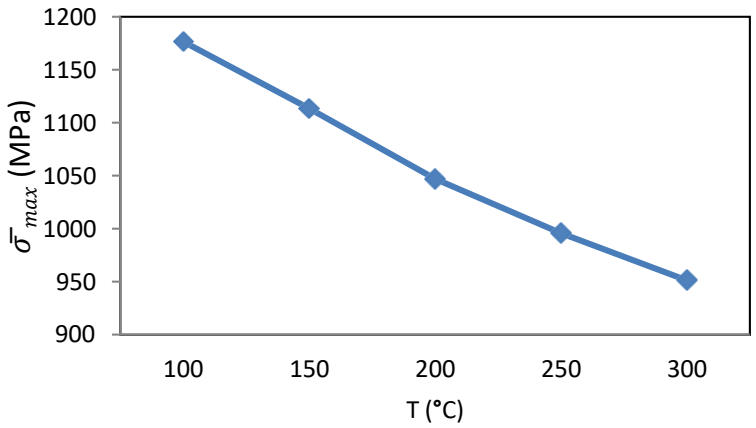

Figure 13. Influence of the temperature on the sleeve maximum effective stress.

Another effect observed on the extruded part is that as friction increases, the maximum effective stress on the core decreases, as shown in Figure 14.

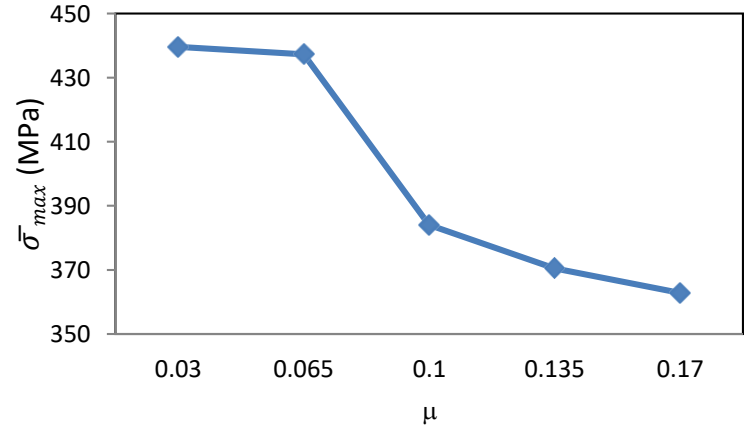

Figure 14. Influence of the friction on the cores maximum effective stress (T = 200 °C).

3.2.6. Die Semi-Angle

Die semi-angle is the most relevant factor to obtain a small extrusion force. The conclusion that can be obtained from the graph in Figure 10f is that there is an optimal value where the extrusion force is minimal; this value has been set at 30°. From this optimal value, the extrusion force increases as the extrusion semi-angle increases or decreases and allows identifying a situation of minimum energy.

3.3. Other Factors Related to the Quality of the Extrudate: Damage Factor

The entire DOE has been done considering the extrusion force as a dependent variable, since this technological parameter is directly related to the power of the extruder to be used and, therefore, will have a direct impact on the investment to be made for the purchase of the equipment; but also, the required forces are close related to the efficiency of the process and, consequently, to the environmental impact of the extrusion process itself. There are other aspects concerning the quality of the final part obtained that can also be analyzed by Finite Element analysis. It is the case of the residual

stresses and the damage induced in the workpiece as a consequence of the forming process. High values of damage could lead to fracture of the part during the component service, so the maximum damage at the core (where inner defects such as chevron cracks can appear in extrusion under specific forming conditions) has been studied in all the configurations.

During the simulations carried out, it was found that the damage induced in the core of the part follows the distribution shown in Figure 15.

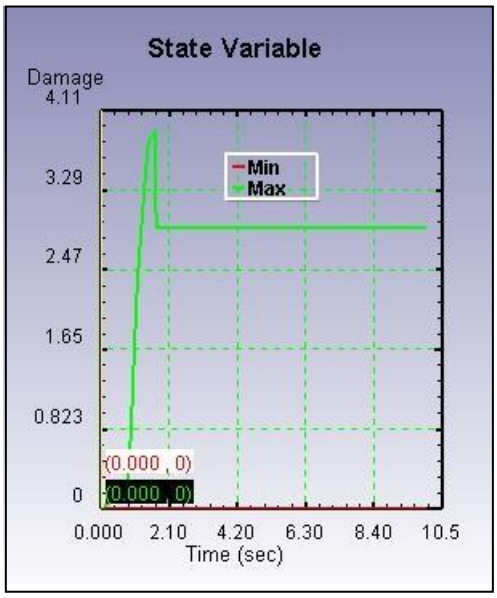

Figure 15. Evolution of damage in the core of the part.

It can be observed that once the damage peak (corresponding to the transient period) is reached, the maximum damage decreases sharply to a value that remains constant throughout the extrusion process, as it reaches a permanent regime.

Taking into account the most influencing factors analyzed, another Taguchi's ANOVA is performed to check their influence in the damage induced in the part. Tables 14 and 15 show the ortogonal array and the results for the average values.

Table 14. Taguchi's orthogonal array for damage factor.

Simulation	Core Diameter (mm)	Friction	Billet Height (mm)	Die Semi-Angle (°)	Damage Factor
1	6	0.07	15	30	0.97
2	6	0.10	20	45	0.76
3	6	0.15	25	60	0.69
4	7	0.07	20	60	1.85
5	7	0.10	25	30	0.53
6	7	0.15	15	45	2.18
7	8	0.07	25	45	2.31
8	8	0.10	15	60	1.62
9	8	0.15	20	30	1.25

Table 15. Taguchi's results for the average values for damage factor.

Level	Core Diameter	Friction	Billet Height	Die Semi-Angle
1	0.81	1.71	1.59	0.92
2	1.52	0.97	1.29	1.75
3	1.73	1.37	1.18	1.39
Delta	0.92	0.74	0.41	0.84
Classification	1	3	4	2

In this case, the order of influence of the factors changes, the core diameter appearing as the most relevant one to obtain a minimum damage value during the process.

3.4. Summary of Most Influential Parameters

According to the results in forces and maximum damage induced in the bimetallic billets, a summary of the most influential parameters in extrusion of these bimetallic components is presented in Table 16.

Table 16. Classification [1] of most influential parameters in extrusion of bimetallic parts (AZ31B core and Ti6Al4V sleeve).

Output Variable	Core Diameter	Friction at Sleeve-Container/Die Interface	Billet Height	Die Semi-Angle
Extrusion force	4	2	3	1
Damage in the core	1	3	4	2

[1] Note: 1—most influential; 4—least influential.

The most influential parameters, considering both criteria (minimum values of forces and damage), are the die semi-angle and friction at the sleeve-container/die interface, so special attention should be paid to obtain favorable interface contact conditions; followed by the geometrical dimensions of the billet, being the billet height more important when paying attention to the minimum forces, and being the core diameter when considering the minimum damage as the most important criterion. These kind of tables are very useful from a practical point of view, as they can be used as guidelines in process design for engineering applications.

As an example of the simulations preformed, Figure 16 shows the *effective* stress and temperature distribution respectively in the FE model, in di*ff*erent stages of the simulation.

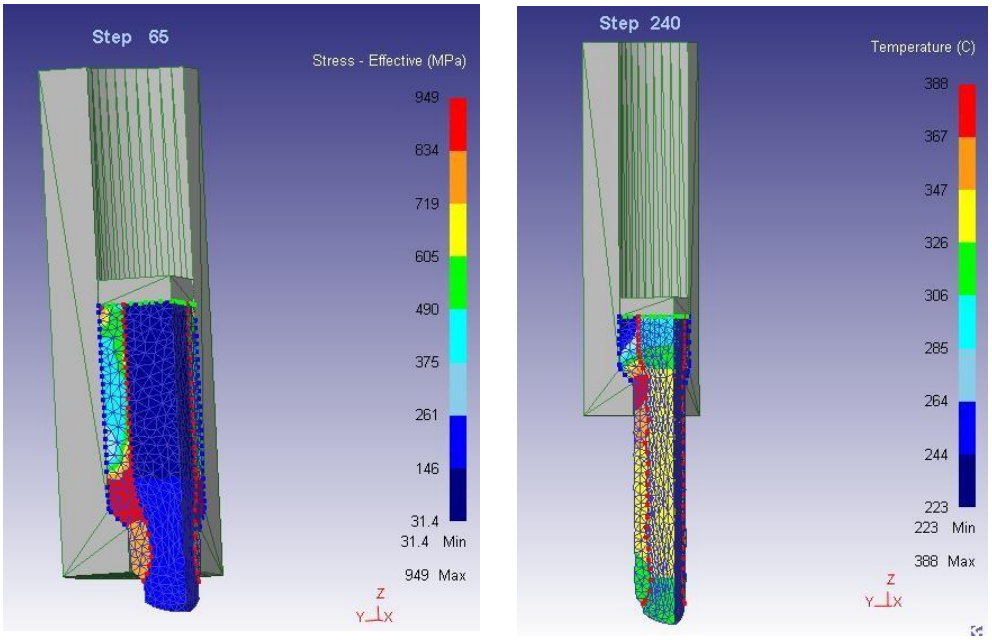

(**a**) (**b**)

Figure 16. Contour diagrams. (**a**) Effective stress distribution during co-extrusion process; (**b**) temperature distribution during co-extrusion process.

4. Conclusions

According to the results presented in this paper, a robust FE model for bimetallic co-extrusion process has been developed. This model represents very accurately the theoretical behavior of a bimetallic cylinder during extrusion process according to Johnson's model.

Using this FE model combined with Taguchi's ANOVA has allowed identifying the most relevant factors in the extrusion force, and in which way this force is a*ff*ected for each of the factors, as shown in Table 13.

Temperature and ram speed have been revealed as the less influence factors in the extrusion force. Regarding ram speed, it has been seen that the higher it is, the lower is the extrusion force needed until it reaches a minimum value from which the extrusion force remains practically constant.

Die semi-angle has been identified as the most critical factor to reduce the extrusion force while the core diameter is the most relevant one to reduce the damage factor in the core component during the process.

During this study die semi-angle of 30° has been proved as the optimum one to reduce the extrusion force during the process.

Friction is found as one of the most relevant factors for both extrusion force and damage factor; however, a balance in the shape factor (ratio between sleeve external diameter and billet height) is also found as key to obtain an extruded part using the minimum extrusion force and with the minimum damage factor.

Finally, this paper describes how the maximum damage in the core component of the billet is influenced by the parameters process and also the damage factor evolution during the co-extrusion process.

The methodology employed in this paper can also be extended to analyze other technological factors; the results of this paper can potentially be used to improve the e*ffi*ciency of this kind of extrusion processes and the quality of the extrudates that, along with the use of lightweight materials, can contribute to sustainable production approaches.

Author Contributions: Conceptualization, D.F., A.R.-P., and A.M.C.; methodology, D.F.; formal analysis, D.F., A.R.-P., and A.M.C.; investigation, D.F., A.R.-P., and A.M.C.; resources, A.R.-P. and A.M.C.; writing—original draft preparation, D.F.; writing—review and editing, A.R.-P. and A.M.C.; supervision, A.R.-P. and A.M.C.; project administration, A.R.-P. and A.M.C.; funding acquisition, A.R.-P. and A.M.C. All authors have read and agreed to the published version of the manuscript.

Funding: This research was funded by the Annual Grants Call of the E.T.S.I. Industriales of UNED through the projects of references [2020-ICF04/B] and [2020-ICF04/D].

Acknowledgments: This work has been developed within the framework of the "Doctorate Program in Industrial Technologies" of the UNED. We would like to extend our acknowledgement to the Research Group of the UNED "Industrial Production and Manufacturing Engineering (IPME)".

Conflicts of Interest: The authors declare no conflict of interest.

References

1. European Comission. Horizon 2020 Work Programme 2018–2020 5.ii. Nanotechnologies, Advanced Materials, Biotechnology and Advanced Manufacturing and Processing. Available online: https://ec.europa.eu/research/participants/data/ref/h2020/wp/2018-2020/main/h2020-wp1820-leit-nmp_en.pdf (accessed on 30 October 2019).
2. Rodríguez-Panes, A.; Claver, J.; Camacho, A.M. The influence of manufacturing parameters on the mechanical behavior of PLA and ABS pieces manufactured by FDM: A comparative analysis. *Materials* **2018**, *11*, 1333. [CrossRef] [PubMed]
3. García-Domínguez, A.; Claver, J.; Sebastián, M.A. Optimization methodology for additive manufacturing of customized parts by fused deposition modeling (FDM). Application to a shoe heel. *Polymers* **2020**, *12*, 2119. [CrossRef] [PubMed]
4. Rodríguez-Prieto, A.; Camacho, A.M.; Sebastián, M.A.; Yanguas-Gil, A. Polymers selection for harsh environments to be processed using additive manufacturing techniques. *IEEE Access* **2018**, *6*, 29899–29911. [CrossRef]
5. García-Domínguez, A.; Claver, J.; Camacho, A.M.; Sebastián, M.A. Considerations on the applicability of test methods for mechanical characterization of materials manufactured by FDM. *Materials* **2020**, *13*, 28. [CrossRef]
6. Negendanka, M.; Mueller, S.; Reimers, W. Coextrusion of Mg–Al macrocomposites. *J. Mater. Process. Technol.* **2012**, *212*, 1954–1962. [CrossRef]
7. Thirumurugan, M.; Anka Rao, S.; Kumaran, S.; Srinivasa Rao, T. Improved ductility in ZM21 magnesium-aluminium macrocomposite produced by co-extrusion. *J. Mater. Process. Technol.* **2011**, *211*, 1637–1642. [CrossRef]

8. Gall, S.; Müller, S.; Reimers, W. Aluminum coating of magnesium hollow profiles by using the coextrusion process. *Alum. Int. J.* **2009**, *85*, 63–67.
9. Lehmann, T.; Stockmann, M.; Naumann, J. Experimental and numerical investigations of Al/Mg compound specimens under load in an extended temperature range. *FEM Trans.* **2009**, *37*, 1–8.
10. Lapovok, R.; Ng, H.P.; Tomus, D.; Estrin, Y. Bimetallic copper-aluminum tube by severe plastic deformation. *Scr. Materalia* **2012**, *66*, 1081–1084. [CrossRef]
11. Berski, S.; Dyja, H.; Banaszek, G.; Janik, M. Theoretical analysis of bimetallic rods extrusion process in double reduction die. *J. Mater. Process. Technol.* **2004**, *153–154*, 583–588. [CrossRef]
12. Kocich, R. Deformation behavior of Al/Cu clad composite during twist channel angular pressing. *Materials* **2020**, *13*, 4047. [CrossRef] [PubMed]
13. Rong, W.; Zhang, Y.; Wu, Y.; Chen, Y.; Tang, T.; Peng, L.; Li, D. Fabrication of high-strength Mg-Gd-Zn-Zr alloys via di*ff*erential-thermal extrusion. *Mater. Charact.* **2017**, *131*, 380–387. [CrossRef]
14. Alcaraz, J.L.; Gil-Sevillano, J. An analysis of the extrusion of bimetallic tubes by numerical simulation. *Int. J. Mech. Sci.* **1996**, *38*, 157–173. [CrossRef]
15. Camacho, A.M.; Rodríguez-Prieto, A.; Herrero, J.M.; Aragón, A.M.; Bernal, C.; Lorenzo-Martin, C.; Yanguas-Gil, A.; Martins, P. An experimental and numerical analysis of the compression of bimetallic cylinders. *Materials* **2019**, *12*, 4094. [CrossRef]
16. Behrens, B.A.; Klose, C.; Chugreev, A.; Heimes, N.; Thürer, S.E.; Uhe, J. A numerical study on co-extrusion to produce coaxial aluminum—Steel compounds with longitudinal weld seams. *Metals* **2018**, *8*, 717. [CrossRef]
17. Thürer, S.E.; Peddinghaus, J.; Heimes, N.; Bayram, F.C.; Bal, B.; Uhe, J.; Behrens, B.A.; Maier, H.J.; Klose, C. Lateral angular co-extrusion: Geometrical and mechanical properties of compound profiles. *Metals* **2020**, *10*, 1162. [CrossRef]
18. Avedesiam, M.; Baker, H. *ASM Speciality Handbook. Magnesium and Magnesium Alloys*; ASM International: Novelty, OH, USA, 1999; pp. 3–4.
19. Donachie, M.J. *Titanium. A Technical Guide*; ASM International: Novelty, OH, USA, 1988.
20. Zhang, D.-W.; Ou, H. Relationship between friction parameters in a Coulomb–Tresca friction model for bulk metal forming. *Tribol. Int.* **2016**, *95*, 13–18. [CrossRef]
21. Li, W.-J.; Zhao, G.-Q.; Ma, X.; Gao, J. Flow stress characteristics of AZ31B magnesium alloy sheet at elevated temperatures. *Int. J. Appl. Phys. Math.* **2012**, *2*, 83–88. [CrossRef]
22. Cockcroft, M.G.; Latham, D.J. Ductility and the workability of metals. *J. Inst. Met.* **1968**, *96*, 33–39.
23. Stebunox, S.; Vlasov, A.; Biba, N. Prediction of the fracture in cold forging with modified Cockcroft—Latham criterion. *Procedia Manuf.* **2018**, *15*, 519–526. [CrossRef]
24. Johnson, W. The pressure for the cold extrusion of lubricated rod through square dies of moderate reduction at slow speeds. *J. Inst. Met.* **1957**, *85*, 403–408.
25. Amigo, F.; Camacho, A.M. Reduction of induced central damage in cold extrusion of dual—Phase steel DP800 using double—Pass dies. *Metals* **2017**, *7*, 335. [CrossRef]
26. García, A.; Claver, J.; Camacho, A.M.; Sebastián, M.A. Comparative analysis of extrusion processes by finite element analysis. *Procedia Eng.* **2015**, *100*, 74–83. [CrossRef]
27. Gisbert, C.; Bernal, C.; Camacho, A.M. Improved analytical model for the calculation of forging forces during compression of bimetallic axial assemblies. *Procedia Eng.* **2015**, *132*, 298–305. [CrossRef]
28. Kumar, T.B.; Panda, A.; Kumar Sharma, G.; Johar, A.K.; Kar, S.K.; Boolchandani, D. Taguchi DoE and ANOVA: A systematic perspective for performance optimization of cross-coupled channel length modulation OTA. *AEU Int. J. Electron. Commun.* **2020**, *116*, 153070. [CrossRef]